Supporting Information for

Controllable Thickness Inhomogeneity and Berry Curvature Engineering of Anomalous Hall Effect in SrRuO$_3$ Ultrathin Films

Lingfei Wang,*[†,‡,⊥], Qiyuan Feng,[‖,§,⊥], Han Gyeol Lee,[†,‡] Eun Kyo Ko,[†,‡] Qingyou Lu,*[‖,§] and Tae Won Noh*[†,‡]

[†]Center for Correlated Electron Systems (CCES), Institute for Basic Science (IBS), Seoul, Republic of Korea

[‡]Department of Physics and Astronomy, Seoul National University, Seoul, Republic of Korea

[‖]Anhui Province Key Laboratory of Condensed Matter Physics at Extreme Conditions, High Magnetic Field Laboratory, Chinese Academy of Sciences, Hefei, Anhui, China.

[§]Hefei National Laboratory for Physical Sciences at the Microscale, University of Science and Technology of China, Hefei, Anhui, China.
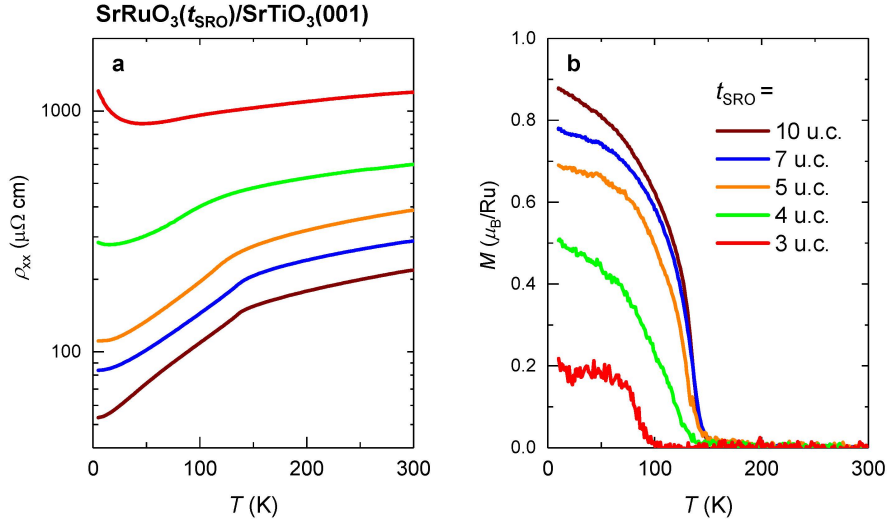
Content

Figure S1. Longitudinal transport and magnetism of SrRuO$_3$ (SRO) films with various thicknesses. (a) Temperature-dependent longitudinal resistivity (ρ_{xx}–T) curves measured from SRO films with various film thicknesses (t_{SRO}). The films were grown on SrTiO$_3$(001) [STO(001)] substrate. (b) T-dependent magnetization (M–T) curves measured from SRO films with various t_{SRO}. Here the nominal t_{SRO} values are all integers. The metallicity and ferromagnetism decay gradually as t_{SRO} decreases.
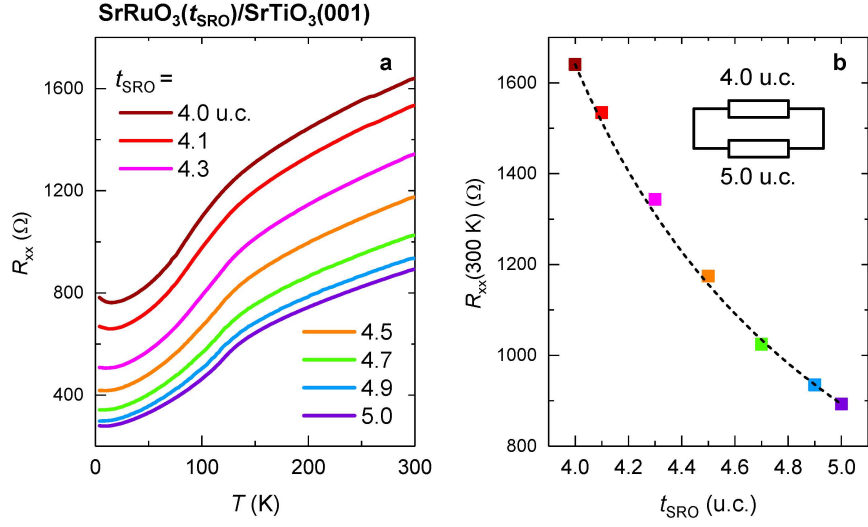
Figure S2. Longitudinal transport of SRO films with inhomogeneous t_{SRO}. (a) T-dependent longitudinal resistance (R_{xx}–T) curves measured from SRO films with non-integer t_{SRO} ranging from 4.1 to 4.9 u.c. All the films were patterned into a 50×50 μm^2 Hall bar. (b) t_{SRO}-dependent R_{xx} at 300 K. The R_{xx} versus t_{SRO} curve can be well reproduced by a fitting curve which considers the resistance of 4.0 and 5.0 u.c.-thick regions are connected in parallel. This fitting result further attests our ability to achieve sub-unit-cell control of t_{SRO}.
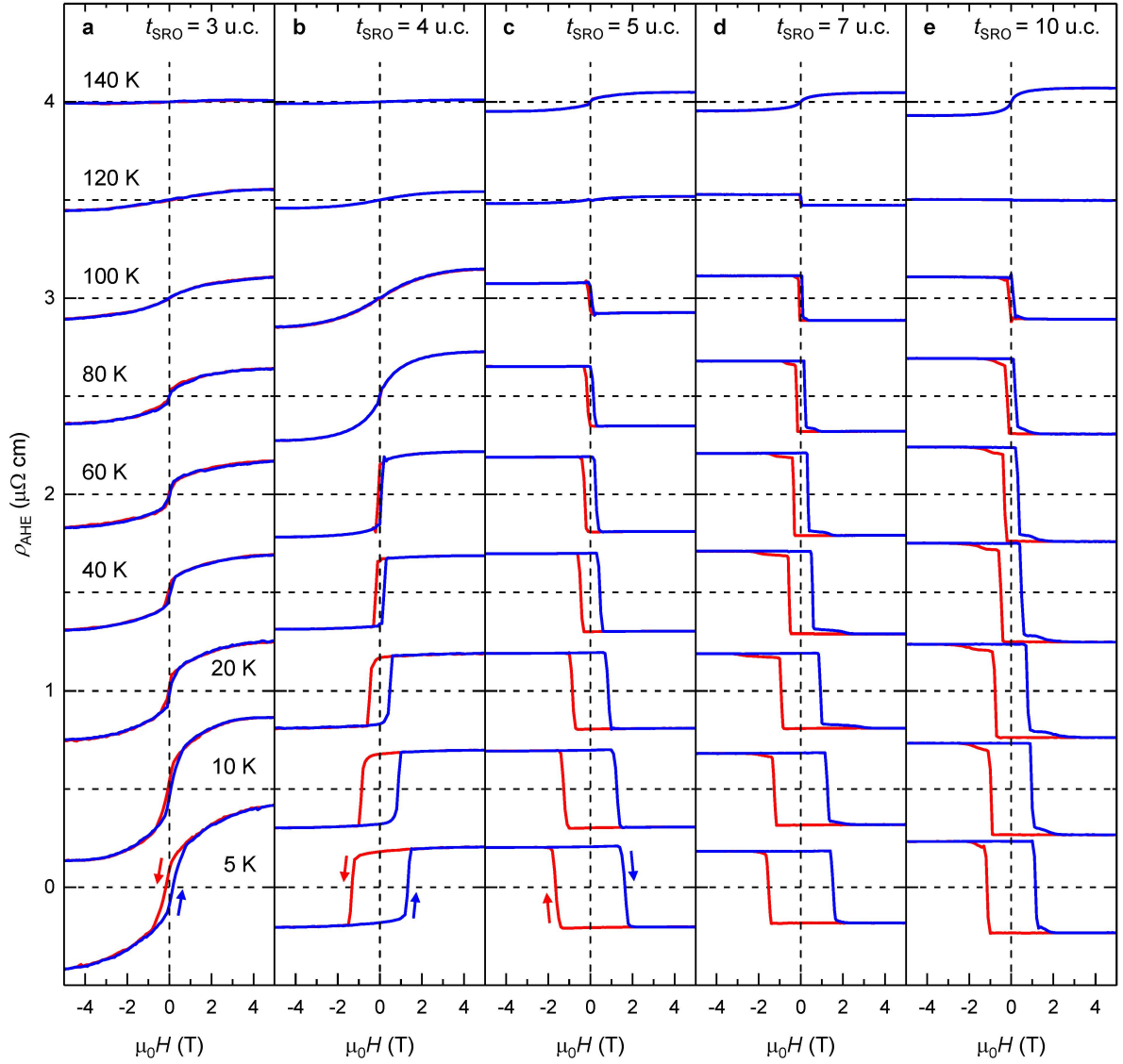
Figure S3. Anomalous Hall effect (AHE) of SRO films with various t_{SRO} and T. (a-e) Magnetic field-dependent anomalous Hall resistivity (ρ_{AHE}-H) curves measured from 3.0 to 10.0 u.c. SRO films at 5 to 140 K. For the films with $t_{SRO} \geq 5$ u.c., a sign reversal of AHE coefficient can be observed as T increases up to 120 ~ 140 K. Note that the 7.0 and 10.0 u.c. SRO films show a two-step magnetic switching. However, these two components do not cause obvious inhomogeneity in k-space Berry curvature. And thus the ρ_{AHE}-H curves do not show any hump-like anomalies.
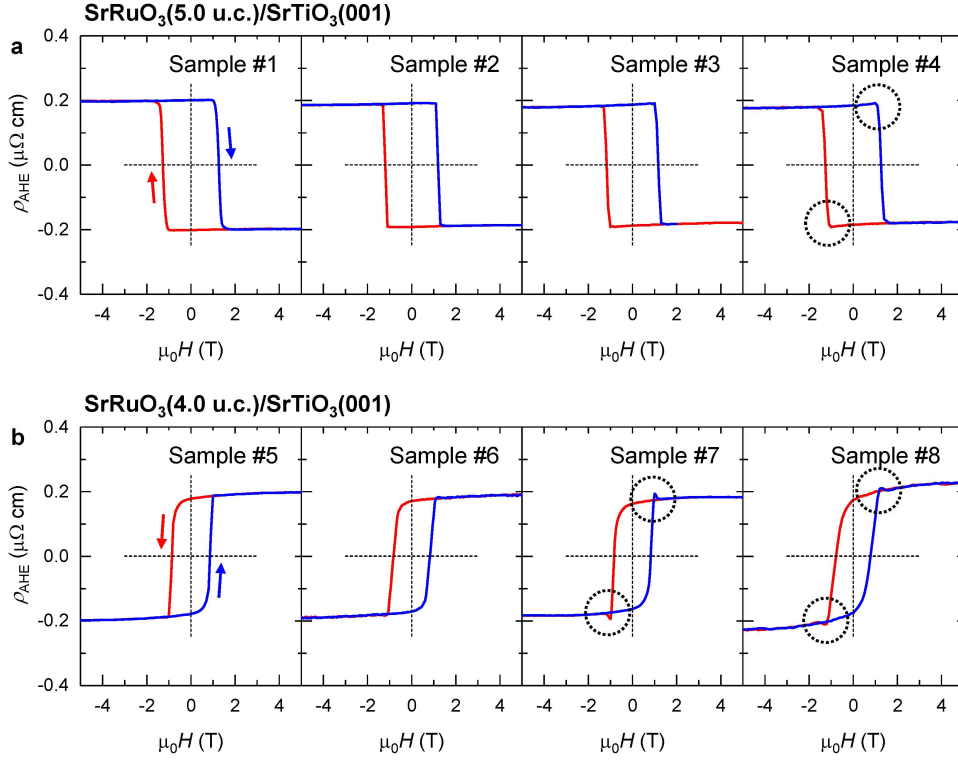
Figure S4. Reproducibility of the ρ_{AHE}-H curves from SRO films with integer t_{SRO}. Inevitable disorders may also induce t_{SRO} inhomogeneity in the SRO films even with integer nominal t_{SRO}. To evaluate the level of t_{SRO} inhomogeneity in these films, we measured the ρ_{AHE}-H curves from four SRO films with t_{SRO} = 5.0 u.c. (a) and 4.0 u.c. (b). The field scanning direction is marked by the solid arrows.

Sample #1, #2, #3, #5, and #6 shows very "clean" ρ_{AHE}-H loops, implying negligible t_{SRO} inhomogeneity. Nevertheless, sample #4, #7, and #8 show tiny humps near the coercive field (marked by the dashed circles). This feature could be assigned to a small t_{SRO} inhomogeneity due to minor disorder or non-uniformity in terrace structure. Note that this hump-like AHE signal is still much smaller than those observed in 4.1 or 4.9 u.c. films. Therefore, we suggest that the t_{SRO} inhomogeneity can be reduced below 10% in our SRO films with integer nominal t_{SRO}.
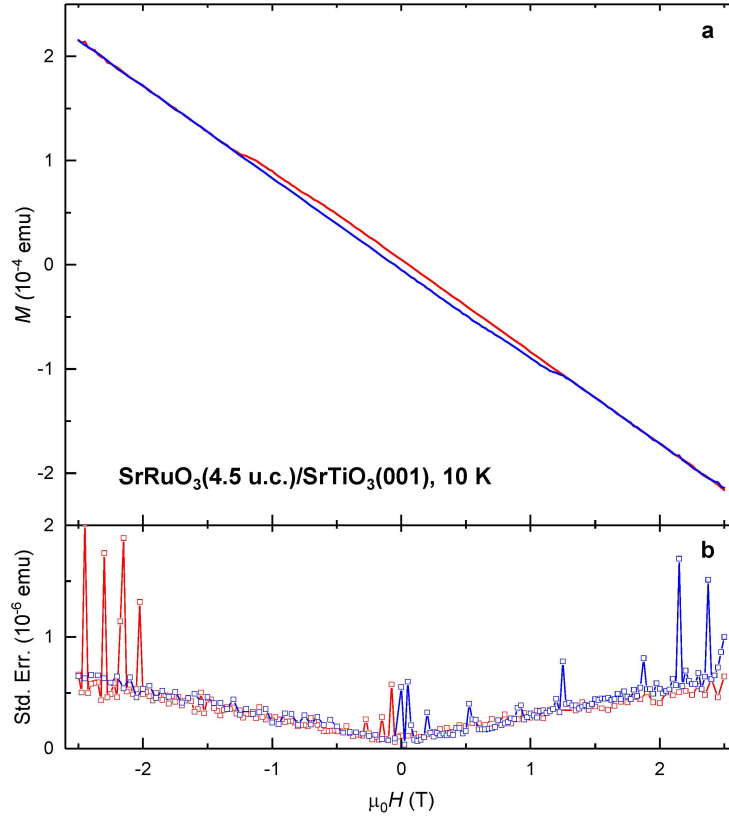
Figure S5. (a) Raw data of the magnetic field-dependent magnetization (*M-H*) hysteresis loop of the SRO(4.5 u.c.)/STO(001) film. The diamagnetic signal from STO(001) substrate makes the *M-H* loop tilt significantly. (b) The standard error (Std. Err.) of the *M* values derived by the MPMS system. Expect for several points at $|\mu_0 H| >$ 2 T, the Std. Err. is smaller than 10^{-6} emu, which is ~1% of the overall *M* signal. Therefore, after subtracting the diamagnetic background, the *M-H* hysteresis loops shown in Figure 5a and Figure S6 still show reasonably small noise level.
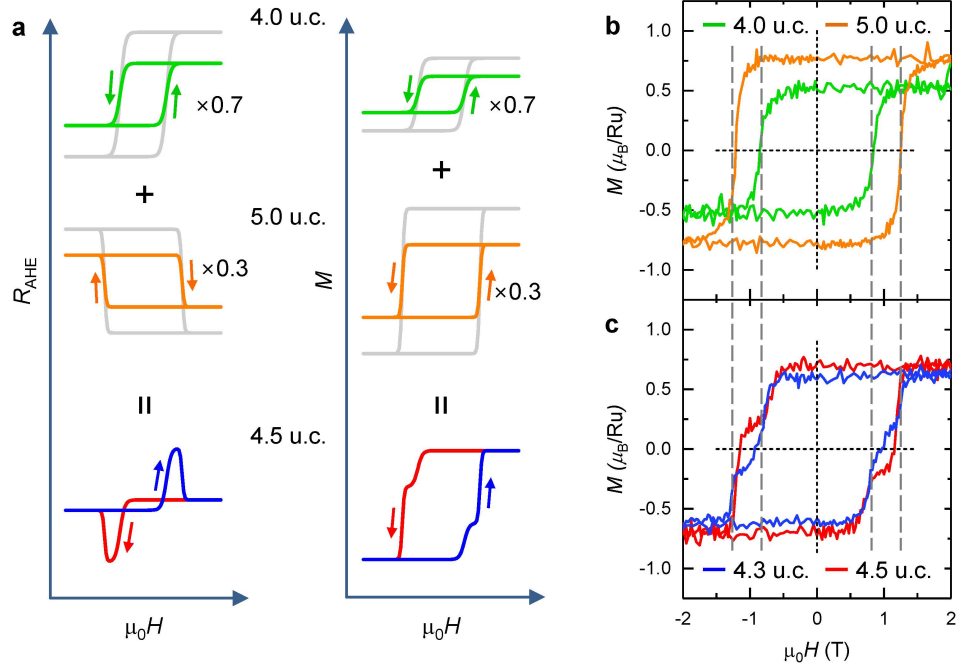
Figure S6. Two-step magnetic switchings in SRO films with inhomogeneous t_{SRO}. (a) Schematic R_{AHE}–H and M–H curves of the SRO film with nominal $t_{SRO} = 4.5$ u.c., which can be seen as a simple superposition of the R_{AHE}–H curves of 5.0 and 4.0 u.c. films. This 4.5 u.c. SRO film should simultaneously exhibit hump-like features in R_{AHE}–H curve and two-step features in the M–H curve. (b) M–H curves measured from the 4.0 and 5.0 u.c. SRO films at 10 K. (c) M–H curves measured from the 4.3 and 4.5 u.c. SRO films at 10 K. The M–H curves clearly exhibit step-like features, and the two H_C show matches well with the H_C values of 4.0 and 5.0 u.c. SRO films.
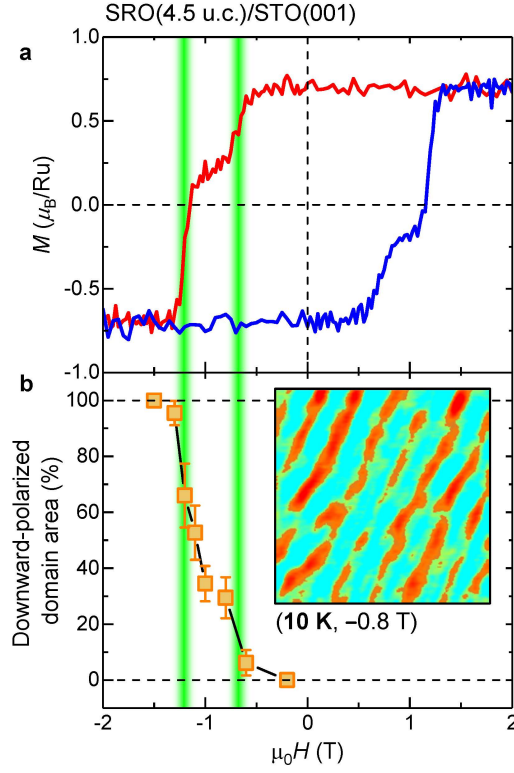
Figure S7. Analysis of magnetic domain configurations during the two-step magnetic switching of the SRO(4.5 u.c.)/STO(001) film. a) *M-H* curve of the SRO(4.5 u.c.)/STO(001) film. b) *H*-dependent downward-polarized domain area, derived from MFM images (Figure 5g-n). The inset is a representative MFM image (measured at 10 K, -0.8 T, shown in Figure 5i) with downward-polarized domains marked in orange color. The increment of downward-polarized domain area clearly exhibits a two-step feature. The two sharp jumps are consistent with the two magnetic switchings observed in the *M-H* curve. On this basis, we confirmed that the MFM result is consistent with the *M-H* loops. They both show clear two-step magnetic switchings rather than one smooth magnetic switching.
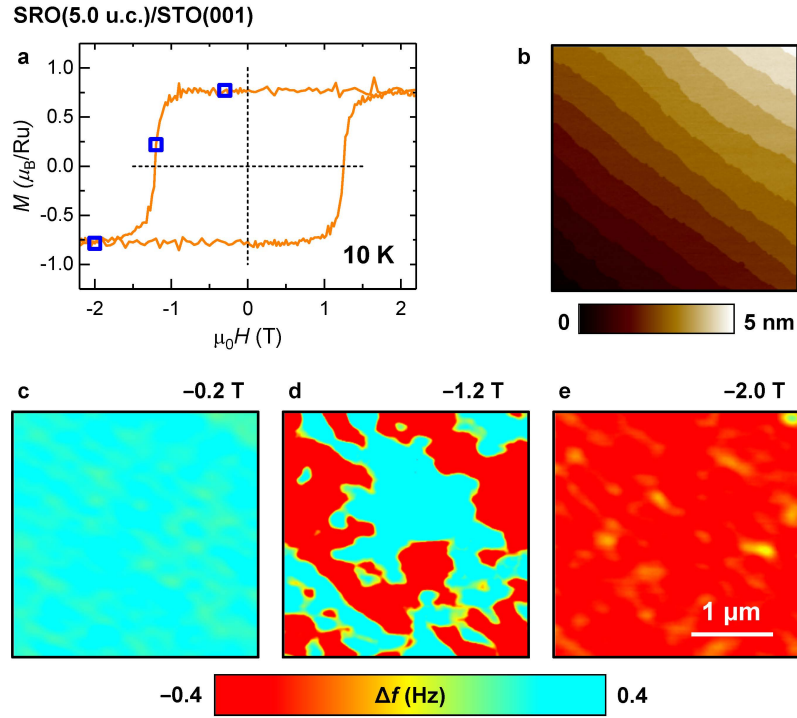
Figure S8. MFM results of the SRO(5.0 u.c.)/STO(001) film. a) *M-H* curve of the 5.0 u.c. SRO film at 10 K. The *H* values for obtaining the MFM images are marked by open squares (blue). b) The AFM topographic image measured from the 5.0 u.c. SRO film. c-e) MFM images measured from the 5.0 u.c. SRO film at 10 K. The scanning areas for all the images are $2.5 \times 2.5 \ \mu m^2$. The images at -0.2 and -2.0 T shows uniform MFM signal, while the image at -1.2 T during the magnetic switching shows large-size bubble domains. The images do not show any clear correlation with the surface terraces.
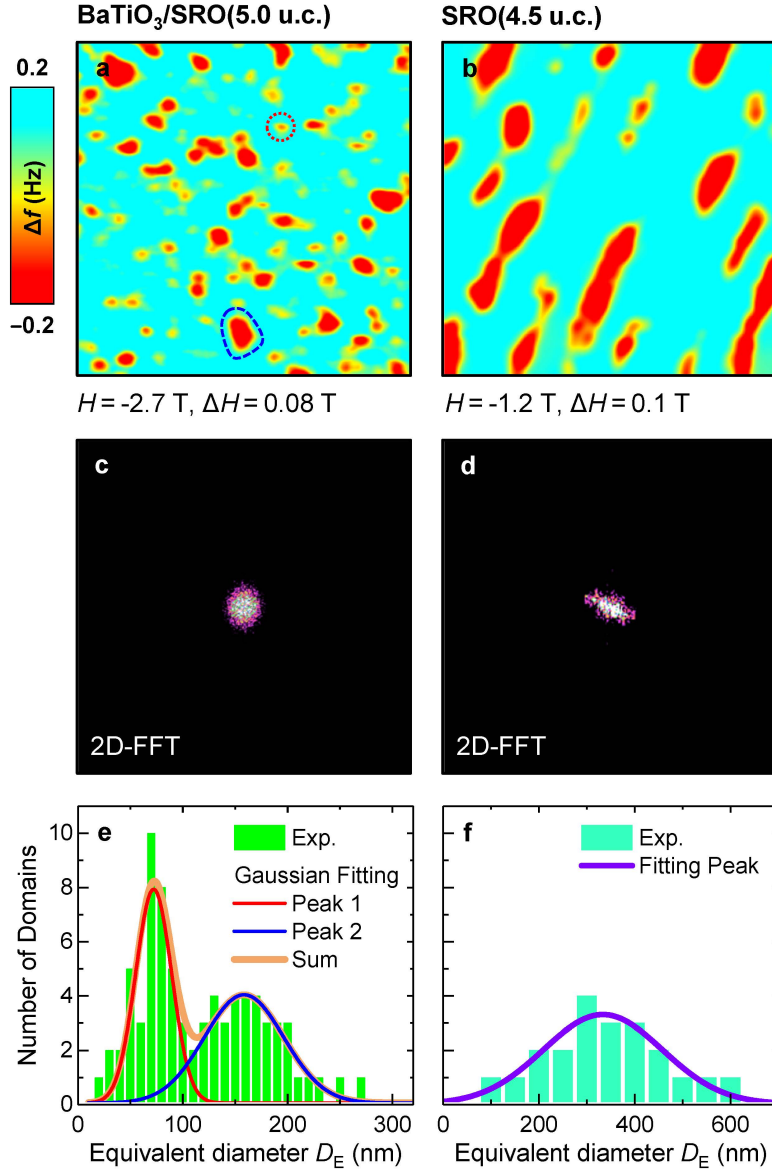
Figure S9. Comparison of the MFM images measured from the $BaTiO_3$/SRO(5.0 u.c.) bilayer and SRO(4.5 u.c.) film. a,b) MFM images after pixel-by-pixel subtraction obtained from the (a) $BaTiO_3$/SRO(5.0 u.c.) film [reproduced data from *Nat. Mater.* **17**, 1087 (2018)] and (b) SRO(4.5 u.c.) film, which are considered to show magnetic skyrmions and thickness inhomogeneities, respectively. The two types of MFM contrasts in (a) are marked by dashed and dotted lines. The scanning areas for both the images are 2.5×2.5 μm². c,d) Two-dimensional fast Fourier transform (2D-FFT) images derived from (a) [(c)] and (b) [(d)]. The circular-shaped contrast in (c) signifies the isotopic nature of the magnetic domains (i.e. irregular-shaped magnetic bubbles and circular-shaped magnetic skyrmions). In contrast, the 2D-FFT image derived from (a) shows a clear anisotropic feature, which further suggests that the thickness inhomogeneity in the 4.5 u.c. SRO film makes the magnetic

domains elongated along the terraces. e,f) Statistical histogram of equivalent domain diameters (D_E) derived from (a) [(e)] and (b) [(f)]. The D_E is calculated by the equation

$$D_E = 2 \left(\frac{domain\ area}{\pi} \right)^{1/2}$$

The histogram in (e) shows two distinct peaks, corresponding to two Gaussian distributions. The sharp peak centered near 90 nm corresponds to the circular-shaped dots with a narrow distribution in size. These MFM contrasts probably originate from magnetic skyrmions, which were expected to have rather uniform sizes. The other broader peak corresponds to either skyrmion clusters or larger magnetic bubbles with irregular shapes and sizes. By contrast, the histogram in (f) shows only one broad Gaussian peak centered at a much larger diameter of ~350 nm. And the number of domains is much smaller than that shown in (e).